ALMA band 10 optics tolerance analysis

M. Candotti[1], Y. Uzawa[1], S. V. Shitov[1], Y. Fujii[1], K. Kaneko[1].

[1]*National Astronomical Observatory of Japan*

2-21-1, Osawa, Mitaka, Tokyo

181-8588,

JAPAN

* Contact: m.candotti@nao.ac.jp, phone +81-422-34-3780

Abstract — **The effects of mechanical tolerances for the cryostat and antenna interface levels and cold optics mechanical structure have been studied in relation to the loss of aperture efficiency and separation angle between the two orthogonal main beams of the ALMA band 10 front-end. Simple ABCD ray tracing method and full electromagnetic physical optics simulations were used to assess the optics performance under misalignment assumptions. As expected, tight tolerances of the cold optics are required for the fulfilment of the ALMA front-end specifications.**

I. INTRODUCTION

The ALMA band 10 Front-End (FE) optical configuration has been designed and theoretically assessed by means of accurate Physical Optics (PO) electromagnetic analysis [1], [2]. The optical design goal was to maximise the overall antenna efficiency and at the same time maintaining the optics structure as simple as possible. In designing the mechanical structure, holding the optical system parts, efforts had to be made to minimise possible deviations from the nominal design. Uncertainties in the mechanical fabrication and assembly process can lead to degradation of the optical front-end performances such as illumination efficiency and orthogonal polarisation beam co-alignment on the sky.

In order to correlate mechanical uncertainties with optical parameter deviations, tolerance analysis techniques can be used. There are different techniques of analysis, each of it combines various uncertainties to get an estimate of the expected optical performance. The worst case analysis consists of simply adding up all of the individual absolute uncertainties to get the worst expected level of performance. This is the most conservative approach, giving the largest possible expected uncertainty values. The root-sum-of-squares (RSS) is based on the fact that the uncertainties are considered normally distributed and independent. Under these assumptions the standard deviation of the resulting distribution is equal to the square root of the sum of the squares of the standards deviations of the initial distributions.

Another popular method of error analysis is the Monte Carlo analysis. With this technique, all uncertainties are characterised by a probability distribution which gives the probability of a certain variable to assume a value within a defined range. For instance a mathematical model is evaluated several times each of it with a new random definition of the uncertainty variables. Each case is a simulation of a possible real case of misalignment. By collecting several simulations (order of 10^3-10^4) allows one to create a statistical distribution of certain output variables. In the contest of this study, the beam separation and the beam tilt at the Focal Plane (FP) can be related to the misalignments characteristic of the system. The assessment of the beam field distribution at the FP by fundamental Gaussian beam analysis gives insights for the allocation of tolerances leading to system performance optimisation and achievement of front-end related ALMA specifications.

In this paper the ALMA specifications closely affected by the tolerance problem are presented. Subsequently, a tolerance study is conducted on the base of simple ray tracing of the optical design and then by PO simulations with the Monte Carlo method. In this analysis, the mechanical assembly error budget assumptions are made and used to statistically describe the errors affecting each of the optical components.

II. ALMA FRONT-END SPECIFICATIONS AND OPTICAL PERFORMANCE REQUIREMENTS

Deviations of the optical system assembly from its nominal configuration arise degradation of the power coupling at the antenna aperture between the illuminating beam and the plane wave representing the incoming radiation from the observed astronomical source. In double orthogonally polarised detector systems, it is also desirable to have the pair of orthogonally polarised main beam simultaneously pointing to the same direction in the sky. Again relative misalignments of optical elements in the FE optical system can induce a beam squint between the two beams when quasi-optical polarisation filtering is applied such as in ALMA band 10. The requirements to be fulfilled in relation the previously described issues are hereby listed:

1) Illumination efficiency

The degradation of the power coupling at the antenna aperture can be due to loss of illumination efficiency that directly relates to an offset illumination of the secondary (truncation at the edge) and/or presence of extra aberrations caused by off-axis mirrors operating at misaligned positions with respect to the nominal optical configuration. Off-axis illumination of the antenna aperture plane also causes non-uniform phase distribution across the primary aperture, that is, loss of power coupling efficiency [3]. Therefore within a first

degree of generalisation, a radial shift at the aperture plane of the illuminating beam can be considered as cause of efficiency degradation. This can also be seen at the focal plane as a tilt of the illuminating beam [3].

Following [3] a maximum drop of efficiency of *1%* is taken into account as a limit of tolerable illumination efficiency loss. In [2], it has been shown that the beam illuminating the sub-reflector has an edge taper of *-12.4dB*. With this illumination distribution at a distance of *5909mm* from the secondary [2], the maximum lateral shift that causes *1%* power coupling efficiency drop with a top-hat field distribution is *41.25mm* (or $0.11R_{sec}$, with R_{sec}=*375mm* [5]). This corresponds to an angular offset from the nominal illumination angle at the focal plane of *0.4°* (*7 mrad*). The effect of on-axis shift of the illuminating beam is not taken into account in this study, since the sub-reflector position can be re-adjusted in order to refocus the whole optical system to optimal antenna focusing configuration [3].

2) Beam separation between the two orthogonally polarised main beams

The on sky co-alignment of the beams of the orthogonally polarised channels shall be less than *10%* of the Full Width Half Maximum (*FWHM*) of the primary beam [4].

A first approximation analysis of the far-field of the main beam *FWHM* can be given by the far-field of a uniform circular field distribution, i.e. the Airy disk *FWHM*:

$$FWHM = 1.02\frac{\lambda}{D_p},$$

where D_p is the primary mirror diameter and λ is the wavelength. The beam squint between the two main beams on the sky can be related to the focal plane through the telescope image scale relation, given by:

$$d_{FP} = \frac{f_e}{206265}\delta\theta_{Bdev} = 0.256mm \div 0.311mm$$

where f_e = *96000mm* is the equivalent focal length for the ALMA Cassegrain antenna [5] and $\delta\theta_{Bdev} = 0.54" \div 0.65"$ are the *10%* of the *FWHM* of the primary beam at *950* and *787GHz* respectively. Therefore, in order to achieve the on sky alignment of the two main beams according to specifications, the beam separation at focal plane should not be more than *0.256mm* and *0.311mm* for the frequencies of *950* and *878GHz* respectively. However this analysis should be considered as guide line. Extra beam squint contributions can arise from the presence of beam aberrations introduced by the telescope system, which can alter the previous results valid for a non diffracted beam.

In the ALMA band 10 optics designs, the cause of beam deviation angle of the two main beams is strictly connected to the two polarisation horns and the grid sub-system alignment accuracy. The two beams following a common optical path after the wire grid element, might however also show extra pointing deviation due to variation on the higher order mode content in their beam pattern field distribution at the focal plane. The use of PO throughout the whole optical system will take into account these extra contributions.

III. Front-end global alignment

The deviation of the FE global alignment (mechanical and optical between antenna and cold optics) from the nominal design is expressed by combination of uncertainties. Uncertainties occur in the manufacturing and assembling of various parts constituting the mechanical structure. Operation factors such as evacuation of the cryostat, cooling down and structural tilts in observational mode also cause deflection of the optical system.

All these uncertainty contributions can be grouped together in order to define a global misalignment error budget. The alignment budget is described by linear and angular factors. The error budget can be separated in two groups: the cryostat and antenna budget and the cold optics budget. Each degree of freedom is thought as a random Gaussian variable which 3σ equals the absolute tolerance parameters listed in table I and II.

A. Antenna and cryostat alignment budget

Table I list the FE interface levels as reported in [6]. For ALMA band 10 the interface levels of concern are:

1. L-a - Antenna flange to FESS (Front-End Support Structure).
2. L-b - FESS to Cryostat.
3. L-c - Cryostat to 4K plate.
4. L-d - Cryostat window angular alignment.
5. L-e - 4K plate to Cold Optics.

The alignment budget (linear and angular) for each interface level is reported in [6, 7], where the system stability due to elevation motion of the antenna and receiver cabin is also taken into account. Table I summarises the FE interface levels, where L-e has been taken from [3].

TABLE I
LINEAR AND ANGULAR ABSOLUTE TOLERANCES FOR CRYOSTAT AND ANTENNA INTERFACE LEVELS [6, 7].

Interface level	Linear [mm]	Angular [°]	Note
L –a	-	0.036	Antenna flange to FSS
L-b	-	0.014	FESS alignment
	-	0.007	FESS to cryostat
L-c	0.689	0.023	Cryostat to 4K plate
L-d	-	0.009	Cryostat window angular alignment
L-e	0.020	0.006	4K plate to cold optics

B. Cold optics alignment budget

The deviation of the cold optics mechanical structure from its nominal design is in principle related to machining precision and mechanical parts assembling. Therefore alignment issues arise in relation to fabrication process and to the adopted mechanical structure design. The fabrication process is characterised by absolute accuracy, meaning that

actual measured numbers are expected to be well within the nominal design length plus/minus a specified range (tolerance τ). Computer numerical controlled milling

TABLE II
LINEAR AND ANGULAR ABSOLUTE TOLERANCES FOR THE COLD OPTICS ELEMENTS

L,	[mm]	τ, [μm]			θτ, [°]
		Milling	Assembling	Total	
Horn	20	20	40	60	0.057
Grid	40	20	40	60	0.057
M1	47	20	40	60	0.045
M2	57	20	40	60	0.040

machines can achieve standard tolerances of ±20μm. Higher level of accuracy can also be achieved, but with an increase of production time. A simple model of defining linear and angular accuracy can result as direct consequence of assuming machining tolerance as absolute uncertainties. That is to say, mechanical parts are characterised by the machining linear accuracy τ, and angular accuracy related to the length of the mechanical part *L*, as shown in Fig. 1. The accuracy of milling an oblique line is related to the linear absolute milling accuracy position within the nominal design. The absolute angle accuracy is then given by θτ.

In the analysis of the mechanical accuracy of the optical system studied in this paper, extra linear inaccuracies are added to the milling ones. This takes into account inaccuracies that arise when the optical parts are assembled together on the Mirror Block (MB). The MB is the mechanical structure where horns, wire grid, mirrors M1 and M2 will be mounted. Table II lists the absolute linear and angular deviations for the model of Fig. 1, where *L* is the length of the optical element along the tangent at the chief ray incident point. The linear tolerances represent a conjunction of milling machine precision and further assembling error of the optical parts. Each degree of freedom is thought as a random Gaussian variable which 3σ equals the absolute tolerance parameters listed in table I and II.

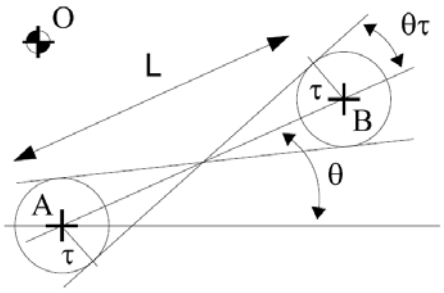

Fig. 1. Simplified model for the absolute angular accuracy of optical elements.

IV. RAY TRACING METHOD

For small linear and angular deviations of the optical elements from the nominal design configuration, the position and tilt of the beam through the optical path can be tracked

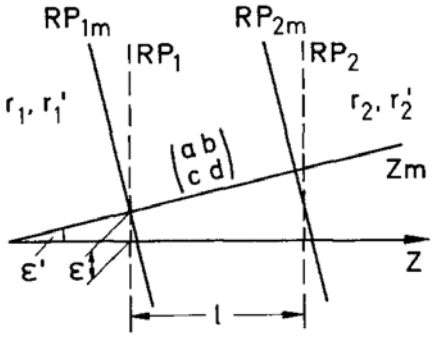

Fig. 2. Misalignment diagram for a forward going system, [REF7].

by ray tracing methods for paraxial beams, as in the case of sub-mm optical systems.

In general linear and/or angular displacements of a single part in the optical system rises a combination of linear and angular displacements in a different location of the system, for example at the focus location of a lens. Therefore when seeking for the total amount of linear displacement at a certain point of the optical path, both contributions coming from linear-to-linear and angular-to-linear relations, are considered. The same concept applies for angular displacements which can be originated from linear and angular displacements of parts in the mechanical system. The ray transfer method used to describe the propagation of a fundamental Gaussian beam for a perfect centred optical system, can be applied to describe misalignments that occur in a optical sub-system where all linear and angular displacements take place on the same plane. Fig. 2 depicts the case of a misaligned forward going system, where r_1, r'_1, r_2 and r'_2 are ray parameters for the incoming and outgoing rays [8]; RP_1 and RP_2 are the aligned reference planes, l is the geometrical distance from RP_1 to RP_2 and *a*, *b*, *c*, and *d* denote the ray transfer matrix elements of this optical system. RP_{1m} and RP_{2m} mean the misaligned reference planes. ε and ε' express the misalignment parameters of this optical system, i.e. distance and slope between the misaligned axis and the ideal axis of this optical system at the input plane [8]. In the paraxial approximation, from geometrical consideration it can be seen that:

$$\begin{bmatrix} r_2 \\ r'_2 \end{bmatrix} = \begin{bmatrix} a & b \\ c & d \end{bmatrix} \cdot \begin{bmatrix} r_1 \\ r'_1 \end{bmatrix} + \begin{bmatrix} \alpha & \beta \\ \gamma & \delta \end{bmatrix} \cdot \begin{bmatrix} \varepsilon \\ \varepsilon' \end{bmatrix}.$$

Where α, β, γ and δ are called misalignment matrix elements determined by:

$$\alpha = 1 - a \quad \beta = 1 - b$$
$$\gamma = -c \quad \delta = 1 - d.$$

If the system depicted in Fig. 2 is a backward going system, then $\delta = 1 - d$ [8]. This is the case of a mirror for example. The linear shift, in the direction of the nominal incident chief ray (Z direction), can also be taken into account. This has

been shown in [3]. Misalignments in the Z direction of an optical part introduce further linear and angular deviations of the propagating ray. This is described by the following matrix notation:

$$\begin{bmatrix} r_2 \\ r'_2 \end{bmatrix} = \begin{bmatrix} a & b & e \\ c & d & f \end{bmatrix} \cdot \begin{bmatrix} r_{1x} \\ r'_1 \\ r_{1z} \end{bmatrix}$$

From geometrical considerations, the misaligned matrices for a plane mirror and a concave mirror (for small ray deviations from the nominal chief ray direction) can be obtained as reported in table III. The wire grid in the ALMA band 10 optics design is modelled as a flat mirror.

TABLE III
MISALIGNED MATRICES FOR RAY TRACING INCLUDING THE Z DIRECTION [3].

Misaligned matrix	Note
$E_{fm} = \begin{bmatrix} 1 & 0 & \sin(2\theta_i) \\ 0 & -2 & 0 \end{bmatrix}$	Flat mirror incident angle θi
$E_{em} = \begin{bmatrix} 1-\cos(2\theta_i) & 0 & \sin(2\theta_i) \\ 1/f & -2 & 0 \end{bmatrix}$	Ellipsoidal mirror incident angle θi and focal length f

V. RAY TRACING MODEL FOR THE ALMA BAND 10 OPTICS

According [1, 2], the optics design make use of a pair of corrugated horns which linearly polarised beams are coupled to the Cassegrain focal plane by means of a wire grid and a pair of ellipsoidal mirrors. Fig. 3 depicts the ALMA band 10 optics scheme for the ray tracing analysis. Details of the design can be found in [2]. The ALMA band 10 optical system is designed in such a way that the P1 polarisation optical path lies on a plane. On the other hand the P0 optical path is divided in to two planes at the level of the wire grid. Therefore the model adopted for the ray tracing analysis, is in somehow different from the original system. In the former model, depicted in Fig. 3, lateral and angular misalignments in the plane normal to the paper are also not considered. In Fig. 3 angular displacements and linear displacements in X and Z are depicted for each optical element. In the ray tracing model each element is subjected to displacement error. Therefore the chief ray is deviated from the nominal path according to the ABCD matrix theory.

Each optical element introduces an error $\boldsymbol{\varepsilon} = [\varepsilon_x \quad \varepsilon \quad \varepsilon_z]^T$ which can be combined into an ABCD matrix expression that keeps trace of the chief ray deviation at the FP. The P0 chief ray deviation at the FP due to the optical displacement errors is described by the following equation:

$$\boldsymbol{r}_{FPP0} = \boldsymbol{M}_{tot}\boldsymbol{r}_{HP0} + \boldsymbol{M}_{tot}\boldsymbol{E}_{HP0}\boldsymbol{\varepsilon}_{HP0} + \boldsymbol{M}_{L4}\boldsymbol{M}_{M2}\boldsymbol{M}_{L3}\boldsymbol{M}_{M1}\boldsymbol{M}_{L2}\boldsymbol{E}_G\boldsymbol{\varepsilon}_G + \boldsymbol{M}_{L4}\boldsymbol{M}_{M2}\boldsymbol{M}_{L3}\boldsymbol{E}_{M1}\boldsymbol{\varepsilon}_{M1} + \boldsymbol{M}_{L4}\boldsymbol{E}_{M2}\boldsymbol{\varepsilon}_{M2}$$

where **M**i are the usual ABCD matrices for a propagation in a uniform medium or focusing elements and $\mathbf{M}_{\mathrm{tot}} = \boldsymbol{M}_{L4}\boldsymbol{M}_{M2}\boldsymbol{M}_{L3}\boldsymbol{M}_{M1}\boldsymbol{M}_{L2}\boldsymbol{M}_{L1}$.

For the P1 polarisation signal:

$$\boldsymbol{r}_{FPP1} = \boldsymbol{M}_{tot}\boldsymbol{r}_{HP1} + \boldsymbol{M}_{tot}\boldsymbol{E}_{HP1}\boldsymbol{\varepsilon}_{HP1} + \boldsymbol{M}_{L4}\boldsymbol{M}_{M2}\boldsymbol{M}_{L3}\boldsymbol{E}_{M1}\boldsymbol{\varepsilon}_{M1} + \boldsymbol{M}_{L4}\boldsymbol{E}_{M2}\boldsymbol{\varepsilon}_{M2},$$

where the contribution of the grid has been left out, since it does not introduce ray deviations for the P1 signal. The previous relations are used to calculate the linear and angular deviations at the focal plane with the statistical methods described in the introduction for the ray tracing method.

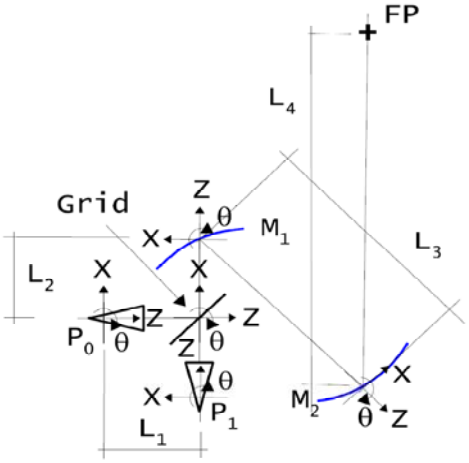

Fig. 3. ALMA band 10 optics schematic describing the ray tracing model.

VI. RAY TRACING ANALYSIS

C. Worst case and RSS

For the Worst Case and RSS error analysis each optical element misalignment parameter is changed at once in the ABCD matrix expressions introduced in the previous section. The resulting linear and angular standard deviations from the nominal chief ray position are then observed at the FP. For the study of the ray tilt due to misalignments, the contributions of all interfaces between the 4K plate and the antenna flange are also considered. The ray tilt analysis at FP is reported in table IV. For the ray separation at the FP the only study of the two horns and wire grid is necessary, since the two rays after the grid are exposed to the same deviation contributions of M1 and M2. Thus keeping the ray separation unchanged from the wire grid to the FP. The separation at the FP for the worst case is then computed by adding the two polarisation's ray linear deviation from the nominal chief ray. The RSS ray separation is computed as the square root of the sum of squares of the P0 and P1 RSS separations from the nominal case, since the separation variable is a result of

linear independent normal distribution random variables. Table IV shows these results.

TABLE IV
WORST CASE AND RSS TILT AND RAY SEPARATION AT FP FOR THE RAY TRACING ANALYSIS OF THE ALMA BAND 10 OPTICS.

	Ray til, [°]		Ray separation, [mm]	
	Worst Case	**RSS**	**Worst Case**	**RSS**
P0	0.436	0.143	0.356	0.150
P1	0.373	0.136		

D. Monte Carlo

By using the same equations for the ray tracing previously described, the displacement errors are now considered simultaneously. The displacement errors are described by random variables with a Gaussian probability distribution function of zero mean and standard deviation such as 3σ equals to the absolute tolerance value listed in table I and II. The 3σ rule ensures 99.73% chances to select a Gaussian random variable within $\pm 3\sigma$ range.

Table V lists the standard deviation for the ray separation and ray tilt of the two polarisation rays at the FP. The results for the ray separation at the focal plane out of $30 \cdot 10^3$ simulations, each of them with a different error misalignment set, are shown in Fig. 4. The output histograms for the ray tilt (not shown here) and rays separation (Fig. 4) are fitted with a Gaussian distribution and a Chi probability distribution respectively. The distribution parameters (i.e. standard deviation and probability of a random variable of falling inside a determined range) are then used to compare with the ALMA specifications introduced in the beginning of this work. For instance the probability of having a ray separation at the FP smaller than *0.257mm* is *0.9477*.

TABLE V
STANDARD DEVIATION OF THE RAY TILT AND RAY SEPARATION BETWEEN THE TWO POLARISATION SIGNAL PATHS OBTAINED FROM MONTE CARLO SIMULATIONS.

Ray tilt, [°]		Ray separation, [mm]
P0	**P1**	
0.136	0.129	0.077

VII. MONTE CARLO ANALYSIS BY MEANS OF PHYSICAL OPTICS ELECTROMAGNETIC SIMULATIONS

The concept of Monte Carlo analysis can be applied to the full 3D geometrical model built with the GRASP software. The optical parts can be displaced relatively to their local Co-ordinate System (CS) that has been carefully chosen in order to represent the final alignment error that occurs in the assembling procedure. The model in GRASP, as depicted in Fig. 5, allows linear displacements along the 3 axis of the local CS and rotation around the principal axis of the single optical parts. For the mirrors and the grid this translates into rotations around the minor and major axis of the surface rim.

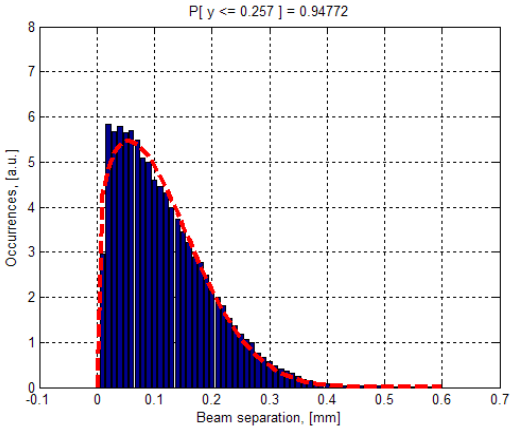

Fig. 4. Ray separation distribution at the focal plane, as a result of ray tracing Monte Carlo simulations over $30 \cdot 10^3$ cases.

The horns are modelled in such a way that they can assume a tilt respect to the cone axis (elevation) in any azimuth direction. All displacements, linear and angular are described as Gaussian random variable according to table II, except for the horn azimuth being described as a random variable of uniform distribution between *-180°* and *180°*. A total of *2000* simulations have been performed for the mirror optical coupling system, each of them characterised by linear and angular displacements at each single optical part. The beam at the focal plane (180mm from M2, [2]) was computed on a grid normal to the chief ray, for each simulation at the lower frequency of Band 10 (*787GHz*), where aberrations are more likely to influence the beam pattern. The two beam polarisation patterns where therefore analysed by means of fundamental Gaussian beam mode fitting procedure. The fundamental Gaussian waist location parameters are used to evaluate the distance between the two polarisation beams at the focal plane. The beam tilt in X and Y gives the beam directions.

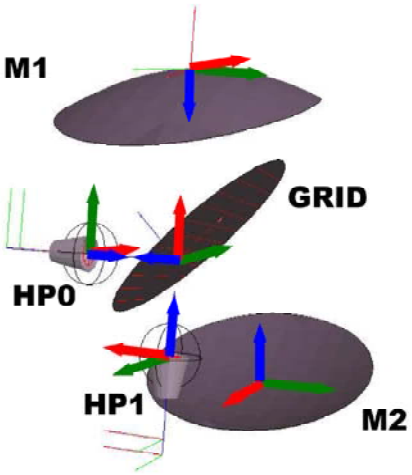

Fig. 5. Local co-ordinate systems of the optics parts for the GRASP Monte Carlo simulation. Red arrow indicates X axis, green arrow stands for Y axis and blue for Z axis. Θ rotation is around Y axis for M1, M2 and grid.

The distance between the fitted Gaussian for the P0 and the P1 beams gives the beam separation at FP. In this work only misalignments of the optics parts are taken into account, no cryostat and other external tilts are hereby considered. The X tilt is on the plane of M1 and M2 and Y tilt is in the plane normal to this. The standard deviation of the beam separation retrievable from the Chi distribution function fitting the beam separation histogram of Fig. 6 is *0.061mm*. From the same histogram the probability of having a beam separation less than *0.31mm* at the focal plane is *0.9954*, over a population distribution of 2000 cases. The standard deviation for the tilt angle of the P0 and P1 beams at the focal plane in the X and Y directions are reported in table VI. Fig. 7 depicts the statistical linear correlation between the beam deviation at the focal plane and each single linear or angular displacement introduced in the 2000 simulated cases for each of the optical elements. The highest correlations are for linear displacements of the two horns and grid along the direction belonging to the plane containing the two horns and the grid, see Fig. 5. Positive displacement of the grid toward the x direction causes deterioration of the beam separation at FP. Similarly, negative displacement in y direction for the P0 horn and x direction for the P1 horn increases the beam separation at FP. If the grid gets closer to the P0 horn, it also causes beam separation at FP. As expected the beams separation is also sensitive to tilt of the grid around its y axis.

TABLE VI
STANDARD DEVIATION OF THE BEAM TILT AND SEPARATION BETWEEN THE TWO POLARISATION SIGNAL OBTAINED FROM PO MONTE CARLO SIMULATIONS.

Beam tilt, [°]				**Beam separation [mm]**
P0		**P1**		
θ_x	θ_y	θ_x	θ_y	
0.081	0.087	0.078	0.070	0.061

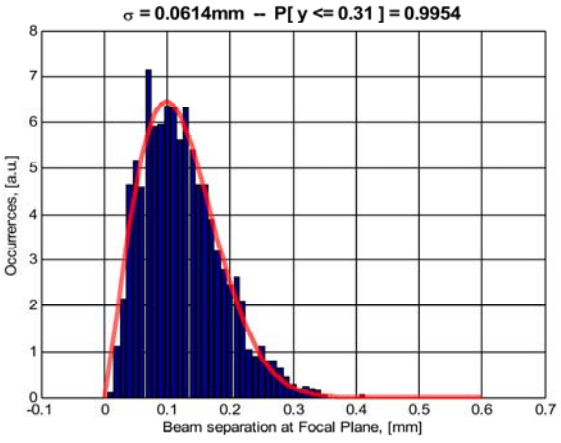

Fig. 6. Beam separation distance at focal plane for 2000 PO simulations.

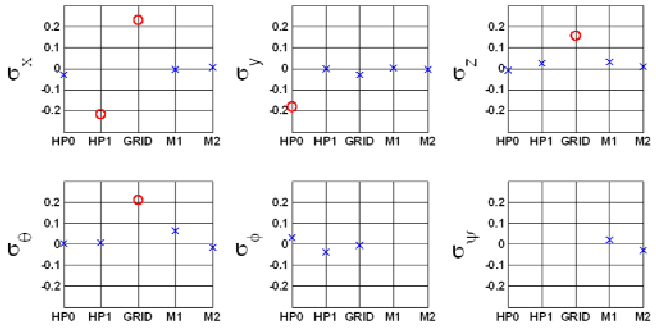

Fig. 7. Linear correlation between the beam separation at FP and error displacement of single optical element. HP0 and HP1 stand for horn P0 and P1, then GRID and mirrors M1 and M2.

VIII. ILLUMINATION EFFICIENCY DEGRADATION

Previously it has been shown that concurrent misalignments of the optical parts translate into beam pointing deviations from the nominal design configuration. In this section selected cases from the PO Monte Carlo simulation are chosen and the beam propagated toward the secondary. The illumination efficiency is then computed with a top hat field distribution of the size of the secondary reflector. The selected cases are those which the fundamental Gaussian fitting analysis gave absolute angular tilts bigger than *0.25*°. For these cases, the illumination efficiency loss with respect to the efficiency evaluated for the nominal optical configuration (i.e. without introducing misalignments) is shown in Fig. 8. The correlation results show that the tilts angle derived from the fundamental Gaussian fitting procedure is not always directly related to the loss of illumination efficiency. The presence of amplitude distortions in the beam patter also causes variations in the illumination efficiency. The drop of illumination efficiency gets to values up to 1% for some of the listed cases, by just considering only optical parts misalignments. Further degradation might be expected if also the operational cryostat tilts will contribute to the total tilt of the receiver system.

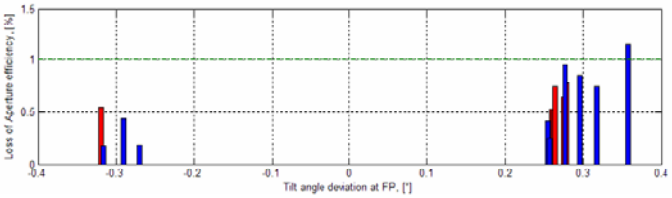

Fig. 8. Drop of illumination efficiency for selected cases where the fundamental Gaussian fitting analysis gave absolute beam tilts in X and Y bigger than 0.25°. The loss of efficiency is this case is only due to the optical part misalignments; the cryostat tilt contributions are not considered here.

IX. CONCLUSIONS

In this paper the effect of alignment displacements of the ALMA band 10 front-end optical parts, has been studied for

the purpose of fulfilling particular optical specifications such as: deviation angle between the two orthogonal polarisation main beams and loss of illumination efficiency at the secondary. These specifications have been addressed and translated to the focal plane interface. The analysis has been carried out by means of different techniques: Worst Case, RSS, and Monte Carlo. A first order study of the beam misalignment at the focal plane followed ray tracing techniques. Monte Carlo statistical analysis was applied to the ray tracing model and also to a more sophisticated model involving 3D full electromagnetic analysis by means of GRASP PO predictions. The general assumption for linear and angular displacements of the optical parts reported in table II, showed that ray tracing RSS analysis gives more pessimistic results compared to the Monte Carlo counterpart.

On the other hand full electromagnetic analysis gave results which show that the beam separation at focal plane can be within the specification of *10%HFBW* for *99%* of the *2000* simulated cases.

However the angular displacement derived by fundamental Gaussian beam mode analysis of the beam pattern at the focal plane, shown to be not fully correlated with the loss of efficiency at the secondary. Aberrations of the amplitude beam pattern at the secondary can also cause drop of illumination efficiency.

It has been shown that loss of efficiency is already reaching values around *1%* for the assumed tolerances in this study. In summary, it seems that as far as concerning the beam separation at focal plane the specifications can be achieved within a *1%* margin in terms of statistical probability. However once the beams propagate through the Cassegrain system they could get further separated due to amplitude distortions at the aperture plane. Illumination efficiency loss is occurring at tilts angles that are less than the upper limit defined by the ray tracing analysis. This result suggests that tighter tolerances should be applied compared to the ones assumed in this work in order to fully meet the specifications.

FUTURE WORK

Further improvements can be considered for the next study of the ALMA band 10 optics. The misalignment errors of the cryostat and antenna levels will be also introduced in the PO calculations. Selected cases might be used to characterise the main beam out of entire PO calculation of the entire optical system including the 12m Cassegrain antenna, therefore validating the study conducted at the focal plane level. Deviation of the cold optics mirror surface parameters due to fabrication process might also be introduced into the statistical description of the optics alignment error budget.

ACKNOWLEDGMENT

The authors would like to acknowledge Y. Sekimoto, A.M. Baryshev and P. T. Peacocke for valuable comments and suggestions.

REFERENCES

[1] K. Murata, *Design of the optics for ALMA 900 GHz band and VSOP-2 40GHz band*, Master thesis, University of Osaka, Japan, 2006.

[2] M. Candotti, Software analysis of the ALMA band 10 optical front-end, Part 1. NAOJ band 10 receiver group internal report, Japan, 2007.

[3] B. Lazareff, Alignment tolerances for ALMA optics, ALMA memo 395, 2007.

[4] C. T. Cunningham, G. H. Tan, H. Rudolf, K. Saini, "Front-end sub-system for the 12m antenna array – Technical specifications," [ALMA-40.00.00.00-001-A-SPE], March 21st, 2007.

[5] V. Gasho, S. Stanghellini, "Technical Specification for the Design, Manufacturing, Transport and Integrationon Site of the 64 ALMA Antennas", ALMA-34.00.00.00-006-A-SPE Version: A, December 15th, 2003.

[6] V. Heinz, "ALMA Mechanical Tolerance Budget", ALMA-80.00.00.00-006-A-REP Version: A, February 28th, 2006.

[7] A. Orlowska, M. Harman, "ALMA Cryostat Tolerance Budget", ALMA-40.03.00.00-033-C-GEN Version: C, January 11th, 2005.

[8] W. Shaomin, *Matrix methods in treating decentered optical systems*, Optical and Quantum electronics, November 29th, 1999.